Pramana – J. Phys. (2022) 96:139
https://doi.org/10.1007/s12043-022-02376-1

Steepening of waves in non-ideal radiative magnetogasdynamic flow with dust particles

ASTHA CHAUHAN[1], ASHISH TIWARI[2], KAJAL SHARMA[2] and RAJAN ARORA[2,*]

[1]Department of Applied Science, The NorthCap University, Gurugram 122 017, India
[2]Indian Institute of Technology Roorkee, Roorkee 247 667, India
*Corresponding author. E-mail: rajan.arora@as.iitr.ac.in

MS received 31 December 2020; revised 8 February 2022; accepted 17 February 2022

Abstract. The singular surface theory is used for the planar and cylindrically symmetric flow of a dusty gas in radiative magnetogasdynamics to study the behaviour of different modes of wave propagation, and their culmination into a steepened form. We have considered one-dimensional steepening of waves. The transport equation for the jump discontinuity in the velocity gradient at the wave heads is determined and solved numerically. The effects of the van der Waals excluded volume of the medium, the mass concentration of solid particles, the ratio of densities, the ratio of specific heats, the radiation parameter and the magnetic field strength on the shock formation are analysed in detail. It is observed that the gradient of density, velocity, pressure and magnetic field are related to each other.

Keywords. Breaking of waves; singular surface theory; radiative magnetogasdynamics; dusty gas.

PACS Nos 02.90.+p; 47.40.Nm; 05.90.+m

1. Introduction

While studying the propagation of a wave in a medium, certain types of discontinuities, such as acceleration waves, shock waves, etc., are encountered. Hence, the mathematicians and physicists pay great attention to the analysis of non-linear systems due to their significant applications in astrophysics. Shock waves have a great scope in the medical field also as they can be used to break the kidney stones of a patient by focussing infinite weak shock waves on that stone. These broken stones can exit from the patient's body through the urinary tract by natural process. Shock waves are also used in the treatment of tendons, ligaments and bones of horses in veterinary medicine. Shock waves have osteogenetic potential and stimulate fracture healing. Shock wave therapy is safe and effective but careless application may cause severe damage. Shock waves are very useful in industrial fields too as they are used for the removal of micron size dust from silicon water surface. They can also be used as wood preservatives, food preservatives, in the extraction of sandalwood oil and in pencil industry. Shock waves can be formed by the steepening of ordinary waves, e.g., ocean waves break on the shore; during supersonic explosions generated by heavy explosives like TNT, which is known as detonations; during the gravitational collapse of large-sized stars into black holes, neutron stars and supernovae; in fluid dynamics during the process of cavitation (when the cavitation bubbles, formed in a liquid, say, by a propeller moving with high speed, get hastily collapsed by the ambient liquid); etc.

A wave may be thought of as a moving surface across which some variables and their derivatives undergo certain discontinuities carried along by the moving surface. The discontinuities are bound to be inter-related across the surface. The relations, which connect the variables and their derivatives on both sides of the discontinuity surface, are known as compatibility conditions. These compatibility conditions form as a result of dynamical conditions. These conditions describe the behaviour of the material medium. The first set of compatibility conditions, termed as Rankine–Hugoniot jump conditions, arises from conservation law applicable over discontinuity surface. The compatibility condition of first-order describes the relation of first-order derivatives. The second or higher-order compatibility condition for a singular surface which describes the relations of derivatives of second or higher order, were first given by Thomas [1] by developing the kinematical and geometrical compatibility conditions for the singular surface. Coleman and Gurtin [2] focussed on how discontinuities grow

Published online: 13 July 2022

and decay. Shyam *et al* [3] studied the singular surface theory when the wave steepened. Chadha and Jena [4] investigated the distinct modes of wave propagation using singular surface theory and compatibility conditions.

The effect of magnetic field on shocks is especially interesting in the context of coronal heating. The temperature of the Sun's corona is substantially higher than that of the surface, which causes this issue. Knowing the physics of the phenomena as well as the effect of magnetic field on a characteristic wave or shock wave is essential. Many researchers have worked on the topic in recent years to understand well the physics of the physical phenomena involved (see [5–8]). The energy transfer through radiation was usually neglected in classical gas-dynamics. However, at high temperature in many phenomena, many investigators have generated a great interest in studying the effects of thermal radiation in gas-dynamics. The gas is likely to be partially ionised at high temperature. Therefore, a complete analysis of such problems is done by simultaneously studying gas-dynamic flow, radiation and electromagnetic fields. Many problems related to radiation effects have been studied by many investigators [9–16] as thermal radiation has a great role in the overall surface heat transfer when the convection heat transfer coefficient is small. Bakier [17] has studied the thermal radiation effects in a porous medium. The study of the radiative magnetogasdynamics is also useful in heating plasma for the controlled thermonuclear devices and the fluctuations in the density in interstellar clouds. Recently, Chauhan [18] obtained self-similar solutions of cylindrical shock waves in a non-ideal radiative gas dynamics in the presence of azimuthal magnetic field using the classical Lie group theoretic approach and discussed the effect of a medium of rotating gas on the flow variables graphically.

The study of fluid flow in a dusty gas is a topic of great interest because of its various applications in environmental and industrial fields such as lunar ash flow, nozzle flow, volcanic explosions, formation of polluted crystals, formation of stars, supersonic flights and various other real-life problems of engineering and science. Several research articles are based on the study of propagation of shock waves in a dusty gas (see [19–25]). The effects of dust particles and radiation heat flux on the propagation of strong shock waves have been studied by Vishwakarma and Patel [26]. They have shown that in the flow field, the flow variables behind the shock got reduced due to the presence of dust particles. Shah *et al* [27] studied the steepened wave for a two-phase flow of chaplygin gas comprising a source term and showed some qualitative features of gas. The behaviour of steepened wave is demonstrated graphically.

In this article, we study a system of non-linear partial differential equations (PDEs) which describes the non-ideal radiative magnetogasdynamic flow under the effect of dust particles. The singular surface theory is used to investigate several aspects of non-linear wave propagation. An overview of this manuscript is as follows: Section 1 presents a brief introduction about shock wave propagation in magnetogasdynamics with thermal radiation effects. In §2, governing equations have been described in detail. In §3, the velocity of the wave propagation and the transport equations have been determined. The nature of velocity gradient has been discussed for a particular case in §4 and 5. The obtained results and a brief conclusion have been given in §6. The effects of dust particles, magnetic field strength, van der Waals gas and radiation parameter on the shock wave propagation are shown. The software package MATLAB is used for the computational work.

2. Governing equations

The system of fundamental/basic equations of motion which governs the motion of one-dimensional radiative magnetogasdynamic flow is given as [10]

$$\begin{aligned}
&\rho_t + \rho u_x + u\rho_x + \frac{\rho u}{x} = 0,\\
&u_t + uu_x + \frac{1}{\rho}\left(p_x + h_x + \frac{2nh}{x}\right) = 0,\\
&p_t + up_x + \rho a^2\left(u_x + \frac{u}{x}\right) + \frac{(\Gamma-1)(1+\tilde{b}\rho)Q}{(1-\xi\rho)} = 0,\\
&h_t + uh_x + 2hu_x + \frac{2h(1-n)u}{x} = 0. \qquad (1)
\end{aligned}$$

In the above system, we have $h = \mu H^2/2$, where H is the transverse magnetic field and μ is the magnetic permeability. n assumes the values 0 and 1 for the axial and the azimuthal magnetic fields, respectively. Gas pressure is denoted by p, density by ρ, γ is the adiabatic index, t denotes the time and x denotes the spatial coordinate. Q denotes the energy dissipation rate by gas per unit volume caused by radiation. Q is defined as $Q = 4\alpha\sigma(T^4 - T_0^4)$, where α denotes the Planck mean absorption coefficient. The value of α depends on temperature T and density ρ. Stefan–Boltzmann constant is denoted by σ and some reference temperatures are shown by T_0. The additional energy gain $-4\alpha\sigma T_0^4$, has been added to $4\alpha\sigma T^4$ (energy loss) due to radiating gas. There is no energy exchange with the boundary wall with constant temperature T_0. For the gas having small dust particles, the value of a^2, the equilibrium speed of

sound in a mixture, is as follows:

$$a^2 = \left[\frac{(\Gamma - \tilde{b}\xi\rho^2 + 2\Gamma\tilde{b}\rho + (\Gamma-1)\tilde{b}^2\rho^2)p}{(1-\xi\rho)(1+\tilde{b}\rho)\rho}\right], \quad (2)$$

where $\tilde{b} = b(1-k_p)$. Here b denotes van der Waals excluded volume. Also,

$$p = \frac{(1-k_p)(1+\tilde{b}\rho)}{(1-Z)}\rho RT, \quad (3)$$

is the equation of state, where R and T represent the specific gas constant and temperatures, respectively. The mass fraction of the solid particles in the mixture is $k_p = m_{sp}/m_g$ and the volume fraction of the solid particles in the mixture is $Z = V_{sp}/V_g$.

Gruneisen coefficient is denoted by Γ and defined as

$$\Gamma = \gamma\frac{(1+\chi\beta)}{1+\chi\beta\gamma},$$

where $\chi = k_p/(1-k_p)$ and β is the ratio of specific heat of solid particles to the specific heats of gas at constant volume. $\xi = k_p/\rho_{sp}$, where ρ_{sp} is the species density of solid particles. The entities Z and k_p are related as $Z = \omega\rho$, where $\omega = k_p/\rho_{sp}$. We also have the equation (see [28])

$$Z = \frac{k_p}{(1-k_p)G + k_p},$$

where the ratio of the density of the solid particles to the species density of the gas is $G = \rho_{sp}/\rho_g$.

3. Derivation of the transport equation

We consider the equation of the wave front ζ as

$$x = X(t), \quad (4)$$

across which the flow variables ρ, u, p and h are continuous, while their derivatives can have discontinuities. Let the flow variables be represented by A and $W = \mathrm{d}X/\mathrm{d}t$ is the propagation speed of ζ. On ζ, the quantities B and $\tilde{B}$ are also defined. Then for a singular surface, kinematical and geometrical compatibility conditions of the first and second orders are as follows:

$$|[A_x]| = B, \quad |[A_t]| = -WB, \quad |[A_{xx}]| = \tilde{B},$$
$$|[A_{xt}]| = W\left(\frac{\partial B}{\partial x} - \tilde{B}\right). \quad (5)$$

Here, $|[A]| = A - A_0$ shows the jump in variable A across the surface ζ, where A and A_0 denote the values just behind the wavefront ζ and just ahead the wave front ζ, respectively. Now, evaluating eq. (1) on the inner boundary of ζ, we get

$$(W-u_0)\eta = \rho_0\lambda, \quad (W-u_0)\rho_0\lambda = \tau + \theta,$$
$$(W-u_0)\tau = \rho_0 a_0^2\lambda, \quad (W-u_0)\theta = 2h_0\lambda, \quad (6)$$

where

$$|[\rho_x]| = \eta, \quad |[u_x]| = \lambda, \quad |[p_x]| = \tau, \quad |[h_x]| = \theta. \quad (7)$$

B is positive for an advancing wave. The relationships between λ, η, θ and τ are as follows:

$$W = \rho_0 B_0 + u_0, \quad \lambda = B_0\eta = \frac{B_0\tau}{a_0^2} = \frac{B_0\rho_0\theta}{2h_0}, \quad (8)$$

where

$$B_0 = \left[\frac{1}{\rho_0}\left(a_0^2 + \frac{2h_0}{\rho_0}(1+n\rho_0)\right)^{1/2}\right]. \quad (9)$$

Now, differentiating eq. (1) with respect to x and after that, taking jump across ζ, we get

$$|[\rho_{xt}]| + \rho_0|[u_{xx}]| + 2|[\rho_x u_x]| + u_0|[\rho_{xx}]| + \frac{1}{x}(\rho_0|[u_x]|) + \frac{1}{x}(u_0|[\rho_x]|) = 0,$$

$$|[u_{xt}]| + |[u_x u_x]| + u_0|[u_{xx}]| + \frac{|[p_{xx}]| + |[h_{xx}]|}{\rho_0} - \frac{(|[\rho_x p_x]| + |[\rho_x h_x]|)}{\rho_0^2} + \frac{2n}{\rho_0}\frac{|[h_x]|}{x} - \frac{2nh_0|[\rho_x]|}{x\rho_0^2} = 0,$$

$$|[p_{xt}]| + u_0|[p_{xx}]| + \left(1 + \frac{\rho_0 a_0^2}{p_0}\right)|[u_x p_x]| + \rho_0 a_0^2\left(|[u_{xx}]| + \frac{|[u_x]|}{x}\right) + \frac{p_0 C_0|[u_x\rho_x]|}{(1-\xi\rho_0)^2(1+\tilde{b}\rho_0)^2} + \frac{u_0}{x}\left(\frac{\rho_0 a_0^2|[p_x]|}{p_0} + \frac{p_0 C_0|[\rho_x]|}{(1-\xi\rho_0)^2(1+\tilde{b}\rho_0)^2}\right)$$
$$= \left[\frac{(1+\tilde{b}\rho_0)}{(1-\xi\rho_0)}(Q_\rho)_0 + \frac{Q_0\tilde{b}|[\rho_x]|}{(1-\xi\rho_0)} + \frac{(1+\tilde{b}\rho_0)\xi Q_0|[\rho_x]|}{(1-\xi\rho_0)^2}\right](\Gamma-1)|[\rho_x]|,$$

$$|[h_{xt}]| + u_0|[h_{xx}]| + 3|[u_x h_x]| + 2h_0|[u_{xx}]| + \frac{2h_0(1-n)|[u_x]|}{x} + \frac{2(1-n)u_0|[h_x]|}{x} = 0, \quad (10)$$

where

$$C_0 = (1-\xi\rho_0)(1+\tilde{b}\rho_0)\{2\tilde{b}\Gamma - 2\xi\rho_0\tilde{b} + 2(\Gamma-1)\tilde{b}^2\rho_0\} - \{\Gamma - \tilde{b}\xi\rho_0^2 + 2\Gamma\tilde{b}\rho_0 + (\Gamma-1)\tilde{b}^2\rho_0^2\} \times(\tilde{b} - \xi - 2\tilde{b}\xi\rho_0). \quad (11)$$

Using eqs (7) and (6),

$$|[\rho_{xx}]|=\tilde{\eta}, \quad |[u_{xx}]|=\tilde{\lambda}, \quad |[p_{xx}]|=\tilde{\tau}, \quad |[h_{xx}]|=\tilde{\theta} \tag{12}$$

and

$$\begin{aligned} |[\rho_{xt}]| &= W(\eta_x - \tilde{\eta}), \quad |[u_{xt}]| = W(\lambda_x - \tilde{\lambda}), \\ |[p_x]| &= W(\tau_x - \tilde{\tau}), \quad |[h_x]| = W(\theta_x - \tilde{\theta}), \end{aligned} \tag{13}$$

in eq. (10), we obtain

$$\begin{aligned}
&W(\eta_x - \tilde{\eta}) + \rho_0\tilde{\lambda} + 2(\eta\lambda + \rho_{0_x}\lambda + u_{0_x}\eta) \\
&\quad + u_0\tilde{\eta} + \frac{\rho_0\lambda}{x} + \frac{u_0\eta}{x} = 0, \\
&W(\lambda_x - \tilde{\lambda}) + (\lambda^2 + 2u_{0_x}\lambda) + u_0\tilde{\lambda} + \frac{\tilde{\tau}}{\rho_0} + \frac{\tilde{\theta}}{\rho_0} \\
&\quad - \frac{(\eta\tau + p_{0_x}\eta + \rho_{0_x}\tau)}{\rho_0^2} - \frac{(\eta\theta + h_{0_x}\eta + \rho_{0_x}\theta)}{\rho_0^2} \\
&\quad + \frac{2n\theta}{x\rho_0} - \frac{2nh_0\eta}{x\rho_0^2} = 0, \\
&W(\tau_x - \tilde{\tau}) + u_0\tilde{\tau} + \left(1 + \frac{\rho_0 a_0^2}{p_0}\right)(\lambda\tau + u_{0_x}\tau + p_{0_x}\lambda) \\
&\quad + \rho_0 a_0^2\left(\tilde{\lambda} + \frac{\lambda}{x}\right) + \frac{p_0 C_0}{(1-\xi\rho_0)^2(1+\tilde{b}\rho_0)^2} \\
&\quad \times (\lambda\eta + u_{0_x}\eta + \rho_{0_x}\lambda) + \frac{u_0}{x}\left(\frac{\rho_0 a_0^2\tau}{p_0}\right. \\
&\quad \left. + \frac{p_0 C_0\eta}{(1-\xi\rho_0)^2(1+\tilde{b}\rho_0)^2}\right) \\
&\quad = \left[\frac{-16\alpha_0\sigma T_0^3(T_\rho)_0(1+\tilde{b}\rho_0)}{(1-\xi\rho_0)} + \frac{Q_0\tilde{b}}{(1-\xi\rho_0)}\right. \\
&\quad \left. + \frac{(1+\tilde{b}\rho_0)\xi Q_0}{(1-\xi\rho_0)^2}\right](\Gamma-1)\eta, \\
&W(\theta_x - \tilde{\theta}) + u_0\tilde{\theta} + 3(\lambda\theta + u_{0_x}\theta + h_{0_x}\lambda) + 2h_0\tilde{\lambda} \\
&\quad + \frac{2h_0(1-n)\lambda}{x} + \frac{2(1-n)u_0\theta}{x} = 0.
\end{aligned} \tag{14}$$

As we have

$$\frac{\mathrm{d}X}{\mathrm{d}t} = W = \rho_0 B_0 + u_0,$$

we use eq. (8) in eq. (14) to eliminate $\tilde{\eta}$, $\tilde{\theta}$ and $\tilde{\tau}$. Then, for λ, we get the following transport equation, which is of Bernoulli type:

$$2\frac{\mathrm{d}\lambda}{\mathrm{d}t} + \phi_1\lambda + \phi_2\lambda^2 = 0, \tag{15}$$

where

$$\begin{aligned}
\phi_1 &= \frac{B_0\rho_0}{x} + \frac{2h_0u_{0_x}}{\rho_0 a_0^2} + \frac{\rho_0(1-n)}{x} \\
&\quad + \frac{p_0C_0(u_{0_x} + \rho_{0_x}B_0)}{(1-\xi\rho_0)^2(1+\tilde{b}\rho_0)^2a_0^2} \\
&\quad + \frac{(2h_0u_{0_x} + B_0p_{0_x})}{\rho_0 a_0^2}\left(1 + \frac{\rho_0 a_0^2}{p_0}\right) \\
&\quad + 3u_{0_x} - \frac{(\Gamma-1)}{a_0^2}\left(\frac{Q_0\tilde{b}}{(1-\xi\rho_0)} - \frac{Q_0(1+\tilde{b}\rho_0)2h_0}{(1-\xi\rho_0)^2B_0\rho_0}\right. \\
&\quad \left. + \frac{16(1+\tilde{b}\rho_0)\alpha_0\sigma T_0^3(T_\rho)_0}{(1-\xi\rho_0)}\right) \\
&\quad + \frac{3B_0\rho_0h_{0_x}}{2h_0} - \frac{2u_0(1-n)}{x} + \frac{u_0}{x}\left(\frac{\rho_0 a_0^2}{p_0}\right. \\
&\quad \left. + \frac{p_0C_0}{(1-\xi\rho_0)^2(1+\tilde{b}\rho_0)^2a_0^2}\right), \\
\phi_2 &= 3 + \left(1 + \frac{\rho_0 a_0^2}{p_0}\right) \\
&\quad + \frac{p_0C_0}{(1-\xi\rho_0)^2(1+\tilde{b}\rho_0)^2a_0^2}.
\end{aligned} \tag{16}$$

The amplitude of a discontinuity wave, also renowned as acceleration waves, always follows a Bernoulli-type transport equation. The basic theory of the development of the acceleration wave and its applications can be found in [29–33].

4. Particular case

To evaluate λ, the flow parameters ρ_0, p_0, u_0 and h_0 just ahead of the wave front ζ must be known. We consider the following forms of the flow parameters:

$$\begin{aligned}
&u_0(x,t) = g(t)x, \quad \rho_0 = \rho_0(t), \\
&p_0 = p_0(t), \quad h_0 = h_0(t),
\end{aligned} \tag{17}$$

where the velocity of the particle is linearly dependent on the spatial coordinate at equilibrium state. 'This state can be visualised in terms of atmosphere filled with a gas, which has spatially uniform pressure variations on account of particle motion [34]'. Equation (1) is integrated by using eq. (17), to obtain

$$g(t) = g_{0_c}\{1 + (t - t_{0_c})g_{0_c}\}^{-1}, \tag{18}$$

$$\rho_0(t) = \rho_{0_c}\{1 + (t - t_0)g_{0_c}\}^{-2}, \tag{19}$$

$$h_0(t) = h_{0_c}\{1 + (t - t_{0_c})g_{0_c}\}^{-4}, \tag{20}$$

$$\begin{aligned}
p_0 &= -\frac{(\Gamma-1)(1-\tilde{b}\rho_0)(1+(t-t_{0_c})g_{0_c})Q_0}{(1-\xi)(2k_0^2+1)} \\
&\quad + \frac{p_{0_c}}{\{1+(t-t_{0_c})g_{0_c}\}^{2\rho_0k_0^2}}
\end{aligned} \tag{21}$$

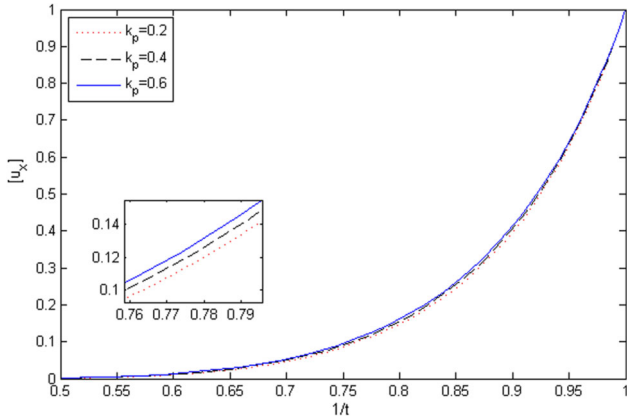

Figure 1. Variation in velocity gradient $[u_x]$ for different values of k_p when $\beta = 1.0$, $G = 1000$, $\rho_{0_c} = 10$, $p_{0_c} = 10$, $h_{0_c} = 0.2$, $b = 0.0009$ and $\gamma = 1.4$.

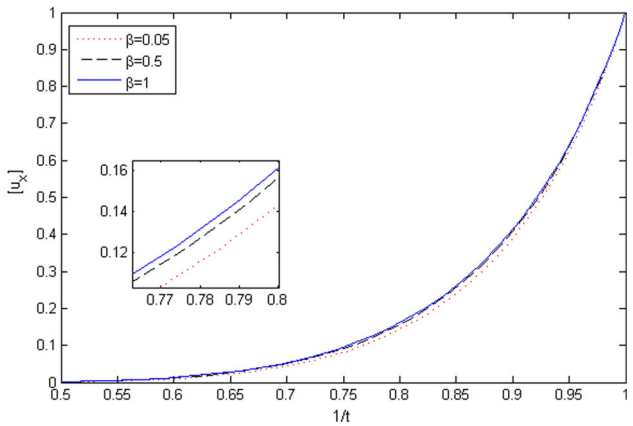

Figure 2. Variation in velocity gradient $[u_x]$ for different values of β when $k_p = 0.6$, $G = 1000$, $\rho_{0_c} = 10$, $p_{0_c} = 10$, $h_{0_c} = 0.2$, $b = 0.0009$ and $\gamma = 1.4$.

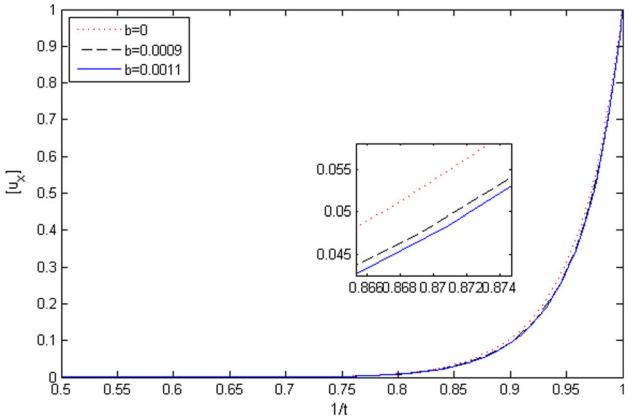

Figure 3. Variation in velocity gradient $[u_x]$ for different values of b when $k_p = 0.6$, $G = 1000$, $\rho_{0_c} = 10$, $p_{0_c} = 100$, $h_{0_c} = 0.2$, $\beta = 1.0$ and $\gamma = 1.4$.

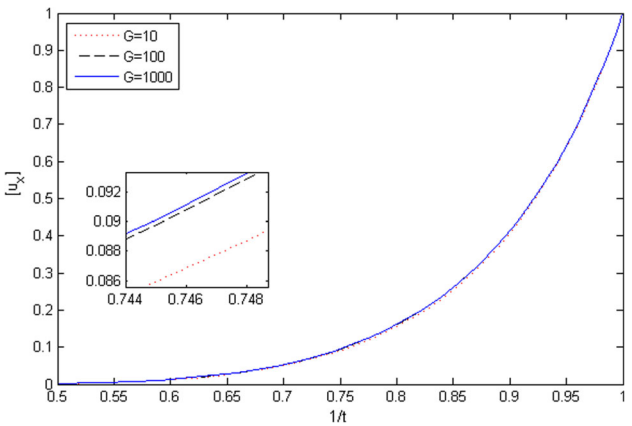

Figure 4. Variation in velocity gradient $[u_x]$ for different values of G when $k_p = 0.6$, $\beta = 1.0$, $\rho_{0_c} = 10$, $p_{0_c} = 10$, $h_{0_c} = 0.2$, $b = 0.0009$ and $\gamma = 1.4$.

where

$$k_0^2 = \left(\frac{(\Gamma - \tilde{b}\xi\rho_0^2 + 2\Gamma\tilde{b}\rho_0 + (\Gamma - 1)\tilde{b}^2\rho_0^2)}{(1 - \xi\rho_0)(1 + \tilde{b}\rho_0)\rho_0} \right)$$

and ρ_{0_c}, g_{0_c}, h_{0_c} are the reference values at $t = t_c$.

5. Behaviour of the velocity gradient

To evaluate the velocity gradient, the dimensionless variables are considered as follows:

$$x_0^* = \frac{x_0}{t_{0_c} a_{0_c}}, \quad t^* = \frac{t}{t_{0_c}}, \quad g^* = g\, t_{0_c},$$

$$\rho_0^* = \frac{\rho_0}{\rho_{0_c}}, \quad \theta^* = \rho_{0_c}\theta, \quad Q_0^* = \frac{Q_0}{\rho_{0_c}}$$

$$T_0^* = a_{0_c}^2 T_0, \quad p_0^* = \frac{p_0}{\rho_{0_c} a_{0_c}^2}, \quad h_0^* = \frac{h_0}{\rho_{0_c} a_{0_c}^2},$$

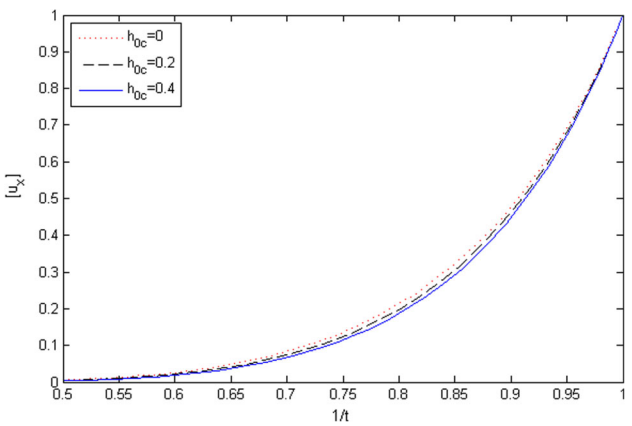

Figure 5. Variation in velocity gradient $[u_x]$ for different values of h_{0_c} when $\beta = 1.0$, $G = 1000$, $\rho_{0_c} = 10$, $p_{0_c} = 1$, $k_p = 0.2$ and $\gamma = 1.4$.

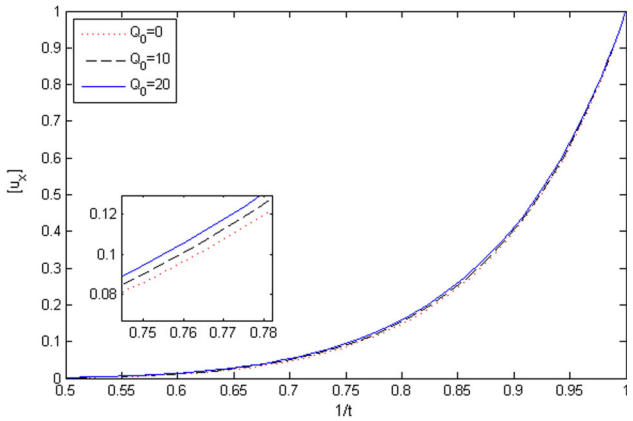

Figure 6. Variation in velocity gradient $[u_x]$ for different values of Q_0 when $\beta = 1.0$, $G = 1000$, $\rho_{0_c} = 10$, $p_{0_c} = 10$, $h_{0_c} = 0$ and $\gamma = 1.4$.

$$a_0^* = \frac{a_0}{a_{0_c}}, \quad b^* = \rho_{0_c} b, \quad \lambda^* = t_{0_c}\lambda. \tag{22}$$

Using (22), we obtain the following transport eq. (15) after suppressing the asterisk sign:

$$2\frac{\mathrm{d}\lambda}{\mathrm{d}t} + \Sigma_1\lambda + \Sigma_2\lambda^2 = 0,$$

where

$$\begin{aligned}\Sigma_1 = {} & B_0\rho_0 + \rho_0 + \left(\frac{2h_0}{\rho_0 a_0^2} + \frac{p_0 C_0}{(1-\xi\rho_0)^2(1+\tilde{b}\rho_0)^2 a_0^2}\right) g(t) \\ & + \frac{2h_0}{\rho_0 a_0^2}\left(1 + \frac{\rho_0 a_0^2}{p_0}\right) g(t) \\ & - \frac{(\Gamma-1)}{a_0^2}\left(\frac{Q_0\tilde{b}}{(1-\xi\rho_0)} - \frac{Q_0(1+\tilde{b}\rho_0)2h_0}{(1-\xi\rho_0)^2 B_0\rho_0}\right. \\ & \left. + \frac{16(1+\tilde{b}\rho_0)\alpha_0\sigma T_0^3 (T_\rho)_0}{(1-\xi\rho_0)}\right) \\ & + g(t) + u_0\left(\frac{\rho_0 a_0^2}{p_0}\right. \\ & \left. + \frac{p_0 C_0}{(1-\xi\rho_0)^2(1+\tilde{b}\rho_0)^2 a_0^2}\right), \\ \Sigma_2 = {} & 4 + \frac{\rho_0 a_0^2}{p_0} \\ & + \frac{p_0 C_0}{(1-\xi\rho_0)^2(1+\tilde{b}\rho_0)^2 a_0^2}. \end{aligned} \tag{23}$$

Integrating eq. (15) with respect to t, we get

$$\lambda = \frac{\lambda_0\Theta_1(t)}{1+\lambda_0\Theta_2(t)}, \tag{24}$$

where $\Theta_2 = \int_{t_0}^{t} \Sigma_1(w)\Theta_1(w)\mathrm{d}w$, $\lambda_0 = \lambda(t_0)$ and $\Theta_1 = \exp(-\int_{t_0}^{t} \Sigma_2(w)\mathrm{d}w)$. From (24), it is observed that $1 + \lambda_0\Theta_2(t) = 0$ at critical time $t = t_c$. Thus, solution (24) breaks down at critical time. This shows the presence of a steepening wave at $t = t_c$, which means that when the initial discontinuity attached with the wave exceeds a critical value of the time, then the compression wave culminates into a shock wave in a finite amount of time. Now, we integrate eq. (24) using eqs (18)–(21) for $1 \le t < \infty$ numerically, to investigate the influence of radiation, van der Waals gas, dust particles and the magnetic field on the jump discontinuity $[u_x]$ for cylindrical motion. Non-magnetic and non-radiative cases are governed by $h_0 = 0$ and $Q_0 = 0$.

The numerical results are consistent with the asymptotic results in the neighbourhood of $t = \infty$ and depicted graphically in figures 1–6. From figures 1–6, it is observed that λ decreases as t increases and tends to zero as t tends to infinity. The velocity gradient decreases as m increases and tends to zero with a faster rate. Figures 1–4 respectively show the effects of parameters k_p, β, b and G on the velocity gradient. An increase in the value of the parameters k_p, β and G gives a rise in velocity gradient λ, and an increase in the value of b causes a decrease in λ. From figure 5, it is observed that an increase in the initial magnetic field leads to a decrease in the velocity gradient λ. Figure 6 indicates that when the rate of energy loss through radiation increases, so does the velocity gradient.

The volume fraction of the dust particle is so small, that the interaction between individual particles can be ignored. Individual flow fields around particles, their collisions, and phase-to-phase heat and mass transfer, as well as momentum exchange, are subject to this restriction. In this context, definite transport processes between dust particles and gas may be treated separately from the overall dynamical problem. This feature has not been discussed much here because it deserves a separate discussion. There may be problems where the distortion of the particle flow field caused by a solid wall or some other particle is the basic physical issue, like particle impact on walls, concentration separation in boundary layers or pipe flow. These issues are beyond the scope of this paper. On the other hand, the behaviour of various wave propagation modes and their culmination into a shock wave can be explored within our current constraints.

6. Results and discussion

In this paper, the evolutionary behaviour of steepened waves in a van der Waals gas containing dust particles with radiative magnetogasdynamics is studied. It is noticed that the gradients of density, velocity, pressure and magnetic field are related to each other. Using

singular surface theory along with the compatibility conditions, the transport equation for jump discontinuity $\lambda = [u_x]$ is determined. The obtained transport equation is of the Bernoulli type that represents the amplitude of an acceleration wave.

From the solution of the obtained transport equation, it is observed that $\lambda(t)$ approaches zero as t approaches infinity for $\lambda_0 > 0$, implying that the shock wave eventually decays and dies out. $\lambda_0 < 0$, on the other hand, implies that solution (24) breaks down at some critical point $t = t_c$, where $1 + \lambda_0\Theta_2(t) = 0$. It is also worth noting that as t rises, profile of the velocity gradient falls significantly and approaches zero as t approaches infinity. The value of λ rises with an increase in the values of k_p, G and β. The value of the non-idealness parameter b decreases as the value of the velocity gradient λ increases. The value of λ reduces as the initial magnetic field and the rate of energy loss by radiation increase.

Our findings are consistent with [19,23] (i.e., an increase in the values of k_p, G and β causes an increase in velocity gradient λ, and an increase in the value of the parameter of non-idealness b causes a decrease in λ. Also, when t approaches infinity, λ tends to zero). This study can be associated with some questions that originate in astrophysical plasmas. It can be important for applications of expanding dusty plasmas in nature, e.g., the dusty layer behind the supernova shock is often found; the aim is to see how the dusty layer is associated with the dust condensation mechanism behind the shock wavefront. Also, our results are consistent with the work of [4,35]. For a mixture (glass or alumina Al_2O_3), the material density of solid particles is $\rho_{sp} = 2.5$ g/cm^3, and the solid particle concentration in the mixture varies between $k_p = 0.2$ and 0.6. One could realise this situation in airflow with alumina or glass particles floating in it. The thickness of the shock wave is of the order of 0.066 μm, which is smaller than the diameter of the solid particles (10 μm). When these solid particles pass through shock fronts, it is logical to think that they are unaffected. Also, particles with a diameter of 1–10 μm relate to interplanetary dust. Particularly, $\gamma = 1.4$ and $\beta = 1$ may correspond to the mixture of glass particles. When $G = 10$, small solid particles in the mixture with a density equal to 10 times that of the perfect gas occupy a significant proportion of the volume, significantly lowering the compressibility of the medium. Further, the compressibility decreases as k_p increases, causing a reduction in shock strength. Small solid particles in the mixture with a density equal to 100 times that of a perfect gas occupy a very small volume when $G = 100$. Consequently, compressibility is not severely decreased, but the inertia of the mixture is significantly increased due to the density of the particles. For $G = 100$, an increase in k_p from 0.2 to 0.4 indicates that the perfect gas in the mixture, constituting 80% of the total mass and 99.75% of the total volume, now constitutes 60% of the total mass and 99.34% of the total volume. For more details, see [36]. The density of the perfect gas in the mixture is much reduced, which overcomes the effect of incompressibility of such a mixture. For $G = 1000$, the similar context can be considered.

Acknowledgements

Astha Chauhan is thankful to the University Grants Commission, New Delhi, for financial support with grant number 2121440656, Ref. No. 21/12/2014(ii)EU-V. Kajal Sharma acknowledges the financial support awarded by the Department of Science and Technology, New Delhi under the scheme Inspire Fellowship.

References

[1] T Y Thomas, *Int. J. Eng. Sci*. **4**, 207 (1966)
[2] B D Coleman and M E Gurtin. *J. Chem. Phys*. **47**, 597 (1967)
[3] R Shyam, L P Singh and V D Sharma, *Acta Astronaut*. **13**, 95 (1986)
[4] M Chadha and J Jena, *J. Comput. Appl. Math*. **34**, 729 (2015)
[5] R Arora, *Comput. Math. Appl*. **56**, 2686 (2008)
[6] S Kuila and T R Sekhar, *Int. J. Appl. Comput. Math*. **3**, 1809 (2017)
[7] B Bira, T R Sekhar and G P Raja Sekhar, *Comput. Math. Appl*. **75**, 3873 (2018)
[8] A Chauhan, R Arora and M J Siddiqui, *Symmetry* **11**, 458 (2019)
[9] G B Whitham, *Linear and nonlinear waves* (John Wiley & Sons, 2011)
[10] V D Sharma, *Int. J. Eng. Sci*. **24**, 813 (1986)
[11] W J Lick, *J. Fluid Mech*. **18**, 274 (1964)
[12] H R Long and W G Vincenti, *Phys. Fluids* **10**, 1365 (1967)
[13] H Schmitt, *ZAMM* **48**, T241 (1968)
[14] V D Sharma, R Shyam and L P Singh, *ZAMM* **67**, 87 (1987)
[15] L P Singh, A Kumar and R Shyam, *Astrophys. Space Sci*. **106**, 81 (1984)
[16] S I Pai, *Magnetogasdynamics and plasma dynamics* (Springer Science & Business Media, 2012)
[17] A Y Bakier, *Int. Commun. Heat Mass Transfer* **28**, 119 (2001)
[18] A Chauhan, *Phys. Fluids* **24**, 017101 (2022)
[19] M Chadha and J Jena, *Int. J. Non Linear Mech*. **74**, 18 (2015)

[20] S K Srivastava, R K Chaturvedi and L P Singh, *Z. Naturforsch. A* **76**, 435 (2021)
[21] L L Tao, L Wei, B Liu, H Zhang and W S Duan, *Pramana – J. Phys*. **95**, 1 (2021)
[22] P K Sahu, *Phys. Fluids* **29**, 086102 (2017)
[23] K Sharma, R Arora, A Chauhan and A Tiwari, *Z. Naturforsch. A* **75**, 193 (2020)
[24] J Yin, J Ding, and X Luo, *Phys. Fluids* **30**, 013304 (2018)
[25] L P Singh, S D Ram and D B Singh, *Acta Astronaut*. **67**, 296 (2010)
[26] J P Vishwakarma and N Patel, *Meccanica* **50**, 1239 (2015)
[27] S Shah, R Singh and J Jena, *Appl. Math. Comput.* **413**, 126656 (2022)
[28] S I Pai, *Pure Appl. Phys*. **3**, 56 (1977)
[29] A Mentrelli, T Ruggeri, M Sugiyama and N Zhao, *Wave Motion* **45**, 498 (2008)
[30] A Jeffrey, *Appl Anal*. **3**, 79 (1973)
[31] G Boillatt and T Ruggeri, *Proc. R. Soc. Edinburgh, Sect. A* **83**, 17 (1979)
[32] A Jeffrey, *Quasilinear hyperbolic systems and waves* (Pitman London, 1976)
[33] W Bleakney and A H Taub, *Rev. Mod. Phys*. **21**, 584 (1949)
[34] V D Sharma, R Ram and P L Sachdev, *J. Fluid Mech*. **185**, 153 (1987)
[35] K Sharma, A Chauhan and R Arora, *Indian J. Phys*. **95**, 1813 (2020)
[36] J P Vishwakarma, G Nath and R K Srivastava, *Ain Shams Eng. J*. **9**, 1717 (2018)